International Journal of Plasticity 52 (2014) 18–32

Contents lists available at SciVerse ScienceDirect

International Journal of Plasticity

journal homepage: www.elsevier.com/locate/ijplas

# Plastic anisotropy of electro-deposited pure α-iron with sharp crystallographic <1 1 1>// texture in normal direction: Analysis by an explicitly dislocation-based crystal plasticity model

Alankar Alankar [a,b,c,*], David P. Field [b], Dierk Raabe [c]

[a] MST-8, Materials Science and Technology Division, MS G755, Los Alamos National Laboratory, Los Alamos, NM 87545, USA
[b] School of Mechanical and Materials Engineering, Washington State University, Box 642920, Pullman, WA 99164, USA
[c] Microstructure Physics and Alloy Design, Max-Planck Institut für Eisenforschung GmbH, 40235 Düsseldorf, Germany

ARTICLE INFO

*Article history:*
Received 12 September 2012
Received in final revised form 5 February 2013
Available online 5 April 2013

*Keywords:*
Crystallographic texture
α-Iron
Dislocations
Kink-pairs
Metal sheet forming

ABSTRACT

We present a single crystal plasticity model based on edge and screw dislocation densities for body centered cubic (bcc) crystals. In a bcc crystal screw dislocations experience high lattice friction due to their non-planar core. Hence, they have much slower velocity compared to edge dislocations. This phenomenon is modeled by accounting for the motion of screw dislocations via nucleation and expansion of kink-pairs. The model, embedded as a constitutive law into a crystal plasticity framework, is able to predict the crystallographic texture of a bcc polycrystal subjected to 70%, 80% and 90% thickness reduction. We perform a parametric study based on the velocities of edge and screw dislocations to analyze the effect on plastic anisotropy of electro-deposited pure iron with long needle-shaped grains having sharp crystallographic <1 1 1>//ND texture (ND: normal direction). The model shows a large change in the *r*-value (Lankford value, planar anisotropy ratio) for pure iron when the texture changes from random to <1 1 1>//ND. For different simulated cases where the crystallites have an orientation deviation of 1°, 3° and 5°, respectively, from the ideal <1 1 1>//ND axis, the simulations predict *r*-values between 4.0 and 7.0 which is in excellent agreement with data observed in experiments by Yoshinaga et al. (ISIJ Intern., 48 (2008) 667–670). For these specific orientations of grains, we also model the effect of long needle shaped grains via a procedure that excludes dislocation annihilation.



## 1. Introduction

During the last two decades efforts were made to explicitly incorporate dislocation density-based constitutive laws into crystal plasticity finite element models e.g. Alankar et al. (2012a, 2009), Aoyagi et al. (2013), Arsenlis and Parks (2002), Arsenlis and Tang (2003), Cheong and Busso (2004), Evers et al. (2004), Erieau and Rey (2004), Lim et al. (2011), Ma et al. (2006), Mayeur et al. (2011), Ortiz et al. (2000) and Shanthraj and Zikry (2011). A detailed review of dislocation density based crystal plasticity models has been done by Roters et al. (2010). While all the aforesaid approaches are phenomenological, some of these use dislocation density as power law dependent variable (e.g. Lim et al. (2011)), the others have them as self sustained geometric loops (e.g. Arsenlis and Parks (2002)). Dislocation density based approach is employed not only for understanding single crystal behavior but also for simulations of polycrystal plasticity. See e.g. Austin and McDowell (2011), Erieau and Rey (2004) and Lim et al. (2011). However, when studying macroscopic plastic anisotropy in metal forming processes, most finite element (FE) approaches use viscoplastic crystal plasticity or even Taylor-based approximations

* Corresponding author at: MST-8, Materials Science and Technology Division, MS G755, Los Alamos National Laboratory, Los Alamos, NM 87545, USA. Tel.: +1 505695 5542; fax: +1 505667 8021.
*E-mail address:* alankar@lanl.gov (A. Alankar).

0749-6419/$ - see front matter © 2013 Elsevier Ltd. All rights reserved.
http://dx.doi.org/10.1016/j.ijplas.2013.03.006

rather than dislocation based constitutive laws. Examples are metal forming simulations based on Taylor-type fixed constraints (FC) type or relaxed constraints (RC) type (Raphanel and Van Houtte, 1985; Van Houtte, 1988; Yoshinaga et al., 2008), or self consistent schemes in conjunction with FEM (Segurado et al., 2012) or viscoplastic crystal plasticity FE models (Beaudoin et al., 1994; Beaudoin et al., 1993; Kalidindi and Schoenfeld, 2000; Neale, 1993; Raabe and Roters, 2004; Raabe et al., 2005; Tikhovskiy et al., 2008; Xie and Nakamachi, 2002; Zhao et al., 2001). Phenomenological approaches e.g. by Yoshida et al. (2007) have been used for showing the effect of crystallographic texture on formability. Constitutive relations used in a number of aforementioned crystal plasticity model use power law based relations between resolved shear stress (RSS) and shear strain rates on slip systems. Such power law based constitutive relations can be fitted extremely well against the experimentally observed stress–strain response of metals in a wide range of temperature and strain rate. However, the effect of dislocation density evolution on the formability of metals is not commonly reported. Moreover, for incorporating fundamentals of microstructure evolution e.g. strength of dislocation reactions based on crystal structures (Alankar et al., 2012b; Devincre et al., 2008; Madec and Kubin, 2003; Queyreau et al., 2009), crystal plasticity models explicitly based on dislocation densities are required (Erieau and Rey, 2004). Here, we demonstrate that by using a crystal plasticity model in conjunction with a novel dislocation-based constitutive model for the prediction of crystallographic texture-related anisotropy, macroscopic forming operations can be understood and designed on a sound microstructural basis. This involves specifically incorporating crystalline plastic anisotropy not only at the kinematic level (texture) but also at the constitutive dislocation behavior level. We show that such dislocation-based crystal plasticity simulation concepts have advantages over conventional viscoplastic methods that require empirical parameters as well as biased or even speculative considerations on internal constraints and micro–macro homogenization.

Most crystal plasticity studies have so far been performed for fcc metals (e.g. Han et al., 2007; Field and Alankar, 2011) and only a few approaches were made to predict specific bcc crystal mechanics (Erieau and Rey, 2004; Lee et al., 1999; Ma et al., 2007; Stainier et al., 2002; Stainier et al., 2003). Some of the published bcc models make no principal difference between the constitutive framework used for fcc crystals and for non-fcc crystals except for the different Schmid factors of the underlying slip systems (Kitayama et al. 2012; Raphanel and Van Houtte, 1985).

In a bcc crystal, {1 1 2} and {1 2 3} slip planes have been reported to be active with <1 1 1> slip directions (Barrett et al., 1937; Gough, 1928). Some studies suggest that only {1 1 0} and {1 1 2} planes play an active role at lower temperatures and {1 2 3} slip occurs only at higher temperatures (Raabe, 1995; Sesták and Seeger, 1978a, 1978b). Other sources indicate that at room temperature only {1 1 0} glide planes are active based on the argument that the slip observed on {1 1 2} and {1 2 3} planes is actually a composite slip on two alternating {1 1 0} planes e.g. Chen and Maddin (1954). Therefore, in this work we use {1 1 0} <1 1 1> and {1 1 2} <1 1 1> slip systems.

Besides these kinematic aspects another key difference between the crystal plasticity of fcc crystals and bcc crystals is that in bcc materials non-Schmid behavior occurs (Taylor, 1928). In the present work we, therefore, focus on bcc metals which show a non-uniqueness of the shear planes associated with a/2 <1 1 1> screw dislocations due to their non-planar core structure which extends into 3 {1 1 0} and 3 {1 1 2} planes that pertain to the same <1 1 1> zone (Ito and Vitek, 2001; Vitek, 1974, 1976). The low energy non-planar core structure causes deep Peierls valleys along the glide direction. For minimizing the energy corresponding to the line length, the screw dislocations hence tend to reside in the form of long segments inside the Peierls valleys (Vitek, 1974, 1976). For the further movement of the screw dislocations, it is necessary that the non-planar cores are constricted in a way that the energy of constriction is in accordance with the Peierls stress required for the motion of screw dislocation. The spread-out core of screw dislocations in bcc metals is responsible for the non-Schmid behavior (Vitek, 1974). Edge dislocations, on the other hand, do not face such a high Peierls stress. Therefore, long screw dislocation lines and short edge dislocation lines are characteristic of bcc metals deformed at moderate and low temperatures (Akhtar and Teghtsoonian, 1975; Cai, 2001). The actual motion of such long screw segments in the presence of high Peierls barriers occurs via the formation and expansion of double kink configurations (Hirth and Lothe, 1992; Seeger and Schiller, 1962). This behavior is common to all bcc metals irrespective of the details of the inter-atomic bonding, owing to the fact that a/2 <1 1 1> screw dislocations are formed along a threefold symmetry axis. Similar behavior has been identified in HCP metals in which screw dislocations on prismatic planes have a non-planar core structure spread out on basal and first order pyramidal planes. The motion of screw dislocations on prismatic and pyramidal planes in HCP crystals can, therefore, also be described via the formation of double kink screw dislocations (Alankar et al., 2011; Monnet et al., 2004; Srivastava et al., 2013).

In this work we present a micromechanical model for bcc crystals considering the individual behavior of screw and edge dislocations, as outlined above. The effect of different edge and screw dislocation kinetics on metal deformation was also pointed out by Stainier et al. (2002). Recently, Acharya and Chapman (2012) have pointed out that there is a strong effect of dislocation structures on the macroscopic plastic anisotropy. We employ the edge and screw dislocation density based constitutive model for analyzing the physical origin of extremely high $r$-values that were observed in electrodeposited <1 1 1>//ND textured pure α-Fe sheets by Yoshinaga et al. (2008). The $r$-value which is also referred to as Lankford value describes the ratio between the in-plane deformation component and the deformation component in through-thickness direction ($r$-value = $\varepsilon_w/\varepsilon_t$). A high $r$-value indicates that material flow occurs primarily parallel to the plane surface in metal forming operations.

A study of $r$-values of electrodeposited <1 1 1>//ND was performed by (Yoshinaga et al., 2008) using a Taylor-based homogenization method (Van Houtte, 1988) for determining the crystalline anisotropy. However, the crystallographic model was not suited to predict the extremely high anisotropy values observed in the experiments (Yoshinaga et al., 2008). We study the effect of different velocities of edge and screw dislocations on the plastic anisotropy of electrodeposited

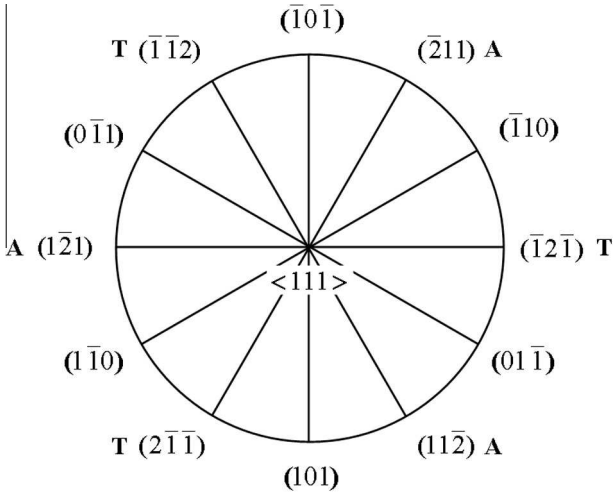


**Fig. 1.** Orientation of the {1 1 0} and {1 1 2} planes that pertain to the same [1 1 1] crystallographic zone. The sense of 'twin' and 'anti-twin' are represented by the symbols 'T' and 'A' respectively. (After Lee et al. (1999)).

<1 1 1>//ND textured pure α-Fe sheets. It enables us to understand and predict the physical processes underlying crystalline anisotropy both from an elementary dislocation level (single slip system behavior) and crystal level (multi slip system behavior; crystallographic texture) perspective. The interaction of these factors (individual dislocation kinetics including differences between screw and edge components; intra-grain multislip conditions; inter-grain constraints) cannot be understood via polycrystal experiments alone. Specifically, by applying the present model to the phenomenon of giant plastic anisotropy, we can demonstrate that the proper incorporation of elementary dislocation kinetic features can have substantial influence on the correct prediction of macroscopic forming characteristics such as deformation-induced plastic anisotropy.

In the following sections we present the constitutive framework, simulation results, discussions and conclusions.

## 2. Constitutive framework

The kinematics of the shear rate on each slip system can be written in terms of a generalized Orowan form. The total plastic shear strain rate is given by (Arsenlis and Parks 2002; Arsenlis and Tang, 2003; Alankar et al. 2009, 2012a; Alankar and Field, 2012):

$$\dot{\gamma}^{\alpha} = b^{\alpha}(\rho_e^{\alpha}\bar{v}_e^{\alpha} + \rho_s^{\alpha}\bar{v}_s^{\alpha})sign(\tau^{\alpha}) \tag{1}$$

where $b^{\alpha}$ is the magnitude of the Burgers vector and $\tau^{\alpha}$ is the resolved shear stress (RSS) on slip system $\alpha$. $\rho_e^{\alpha}$ is the edge dislocation density, $\rho_s^{\alpha}$ is the screw dislocation density, $\bar{v}_e^{\alpha}$ is the average velocity for edge type dislocations and $\bar{v}_s^{\alpha}$ is the average velocity for the screw type dislocations.

Fig. 1 shows the asymmetric arrangement of the slip planes associated with the slip direction <1 1 1>. On {1 1 2} planes the slip resistance along the twin direction is lower than that for slip along anti-twin directions due to the non-Schmid effect in a bcc crystal (Vitek, 1974, 1976). The twin and anti-twin directions are denoted by 'T' and 'A' respectively. The slip systems along with the twin and anti-twin directions are shown in Table 1.

### 2.1. Dislocation multiplication

The rates for the multiplication and annihilation of edge and screw dislocations are adopted from the work of Arsenlis and Parks (2002) and from the work of Alankar et al. (2009, 2011, 2012a). We describe the edge and screw dislocation densities through the expansion of dislocation loops that proceed from Frank-Read sources. This means that the edge dislocation density increases due to moving screw dislocations and the screw dislocation density increases due to moving edge dislocations as given by the following equations:

$$\dot{\rho}_{e,mul}^{\alpha} = 2\frac{\rho_s^{\alpha}\bar{v}_s^{\alpha}}{\bar{l}_s^{\alpha}} \tag{2a}$$

$$\dot{\rho}_{s,mul}^{\alpha} = 2\frac{\rho_e^{\alpha}\bar{v}_e^{\alpha}}{\bar{l}_e^{\alpha}} \tag{2b}$$

where $\bar{l}_e^{\alpha}$ and $\bar{l}_s^{\alpha}$ represent average segment lengths for the edge and screw type dislocations, respectively.

**Table 1**
Slip directions ($\mathbf{m}_0^\alpha$) and slip plane normals ($\mathbf{n}_0^\alpha$) in bcc crystals.

| Slip system ($\alpha$) | ($\mathbf{m}_0^\alpha$) | ($\mathbf{n}_0^\alpha$) | Slip system ($\alpha$) | Label | ($\mathbf{m}_0^\alpha$) | ($\mathbf{n}_0^\alpha$) |
|---|---|---|---|---|---|---|
| 1 | [1 1 1] | $(01\bar{1})$ | 13 | A | [1 1 1] | $(1\bar{2}1)$ |
| 2 | [1 1 1] | $(\bar{1}01)$ | 14 | T | [1 1 1] | $(2\bar{1}\bar{1})$ |
| 3 | [1 1 1] | $(1\bar{1}0)$ | 15 | A | [1 1 1] | $(11\bar{2})$ |
| 4 | $[\bar{1}11]$ | $(\bar{1}0\bar{1})$ | 16 | A | $[\bar{1}11]$ | $(\bar{1}1\bar{2})$ |
| 5 | $[\bar{1}11]$ | $(0\bar{1}1)$ | 17 | T | $[\bar{1}11]$ | $(2\bar{1}\bar{1})$ |
| 6 | $[\bar{1}11]$ | (110) | 18 | A | $[\bar{1}11]$ | $(\bar{1}\bar{2}1)$ |
| 7 | $[\bar{1}\bar{1}1]$ | $(0\bar{1}\bar{1})$ | 19 | A | $[\bar{1}\bar{1}1]$ | $(\bar{1}21)$ |
| 8 | $[\bar{1}\bar{1}1]$ | (101) | 20 | T | $[\bar{1}\bar{1}1]$ | $(\bar{2}1\bar{1})$ |
| 9 | $[\bar{1}\bar{1}1]$ | $(\bar{1}10)$ | 21 | A | $[\bar{1}\bar{1}1]$ | $(\bar{1}\bar{1}2)$ |
| 10 | $[1\bar{1}1]$ | $(10\bar{1})$ | 22 | A | $[1\bar{1}1]$ | $(1\bar{1}2)$ |
| 11 | $[1\bar{1}1]$ | (011) | 23 | T | $[1\bar{1}1]$ | $(21\bar{1})$ |
| 12 | $[1\bar{1}1]$ | $(\bar{1}\bar{1}0)$ | 24 | A | $[1\bar{1}1]$ | (121) |

Slip systems 1 - 12 do not use labels for twin and anti-twin directions viz. A and T.

### 2.2. Dislocation annihilation

Two dislocations of opposite sign annihilate each other when they come within a critical distance. The annihilation rates are given by (Arsenlis and Parks 2002; Arsenlis and Tang, 2003; Alankar et al. 2009, 2011, 2012a):

$$\dot{\rho}^\alpha_{e,ann} = -(\rho^\alpha_e)^2 R^\alpha_e \bar{v}^\alpha_e \tag{3a}$$

$$\dot{\rho}^\alpha_{s,ann} = -(\rho^\alpha_s)^2 R^\alpha_s \bar{v}^\alpha_s \tag{3b}$$

where $R^\alpha_e$ and $R^\alpha_s$ are the critical radii for edge and screw dislocations, below which spontaneous annihilation occurs, respectively. This means that the critical radius is the minimum distance up to which two opposite signed dislocations can approach while gliding on the same plane before they spontaneously annihilate.

For both, edge and screw dislocations, Arrhenius type equations for the velocity are used. The edge dislocations are assumed not to be affected by the Peierls stress. The edge dislocation velocity is given by the equation:

$$\bar{v}^\alpha_e = \bar{v}_{e,0} exp\left(-\frac{F_0}{k_B T}\left(1-\left(\frac{|\tau^\alpha|}{\tau^\alpha_{e,0}+S^\alpha}\right)^{pe}\right)^{qe}\right) \tag{4a}$$

where $\bar{v}_{e,0}$ is a reference velocity for edge dislocations, $F_0$ the free energy of the activation of motion of edge dislocations, $k_B$ the Boltzmann constant, $\tau_{e,0}$ the lattice friction stress acting on edge dislocations and $T$ the absolute temperature. $pe$ and $qe$ are material coefficients such that $0 \leqslant pe \leqslant 1.0$ and $1.0 \leqslant qe \leqslant 2.0$. $S^\alpha$ is the slip resistance and $\tau^\alpha$ is the resolved shear stress on slip system $\alpha$. Due to high Peierls stress acting on screw dislocations, we describe screw dislocation motion in terms of the formation of kink pairs. The velocity of a screw dislocation segment ($\bar{v}^\alpha_s$) is governed by thermally activated nucleation of kink pairs. It is given by Dorn and Rajnak (1964), Duesbery (1969) Guyot and Dorn (1967) Hirth and Hoagland (1993) Tang et al. (1998) Xu and Moriarty (1998):

$$\bar{v}^\alpha_s = b^\alpha \frac{l^\alpha}{l_0}\frac{\upsilon_D b^\alpha}{l_0}\exp\left(-\frac{F_{0,kink}}{k_B T}\left(1-\left(\frac{|\tau^\alpha|}{\tau_P}\right)^{ps}\right)^{qs}\right) \tag{4b}$$

where $F_{0,kink}$ is the free energy of the formation of a kink-pair, $ps$ and $qs$ are material coefficients such that $0 \leqslant ps \leqslant 1$ and $1 \leqslant qs \leqslant 2$. $l^\alpha$ is the length of the straight screw dislocation segment. $l_0$ is the critical length for kink pair nucleation. $v_D$ is the Debye frequency, $\tau_p$ is the Peierls stress, and $b^\alpha$ is the magnitude of the Burgers vector. Stainier et al. (2003) proposed temperature and strain rate dependent constitutive form of Peierls stress. Since, in the present work we performed all the simulations at room temperature, we use a constant value of the Peierls stress. The term $v_D b^\alpha/l_0$ describes the attempt frequency for kink pair formation and the term $l^\alpha/l_0$ describes the number of competing sites for kink pair formation on the segment $l^\alpha$ (Kubin et al., 1998; Tang et al., 1998).

### 2.3. Forest hardening

The slip resistance $S^\alpha$ on a slip system $\alpha$ is given by a modified Taylor type equation (Franciosi et al., 1980) as shown below. The forest hardening is applicable only for edge dislocations in bcc metals since screw dislocations have very low velocity as compared to edge dislocations and do not form a junction with forest dislocations (Monnet et al., 2004). The slip resistance $S^\alpha$ on a slip system $\alpha$ is given by:

**Table 2**
Material constants and parameters for α-Fe used in the current CPFE model.

| | | |
|---|---|---|
| Elastic constants | $C_{11}$ | 236.0 GPa |
| | $C_{12}$ | 134.0 GPa |
| | $C_{44}$ | 119.0 GPa |
| Burgers vector | \|b\| | 2.49 e−9 m |
| Edge dislocation velocity | $pe$ | 0.10 |
| | $qe$ | 1.11 |
| | $\overline{v}_{e,0}$ | 1.0 e−3 m $s^{-1}$ |
| | $F_0$ | 3.0 e−19 J $atom^{-1}$ |
| | $k_B$ | 1.38 e−23 J $K^{-1}$ |
| | $\tau_{e,0}$ | 20 MPa |
| | $R_e$ | 19.0 e−9 m |
| Screw dislocation velocity | $ps$ | 0.71 |
| | $qs$ | 1.71 |
| | $F_{0,kink}$ | 2.8e−19 J $atom^{-1}$ |
| | $\tau_P$ | 370 MPa |
| | $R_s$ | 95.0e−9 m |
| | $\upsilon_D$ | $10^{13}$ $s^{-1}$ |
| | $l_0$ | 1.0 e−6 m |
| Slip system interaction | Self hardening | 0.10 |
| | Latent hardening | 0.14 |
| Mean-free path coefficient | $\lambda$ | 20.0 |

$C_{11}$, $C_{12}$ and $C_{44}$ are elastic constants for α-Fe (Adams et al. (2006)). $\overline{v}_{e,0}$ is the pre-exponential factor in the equation for velocity of edge dislocation. $pe$ and $qe$ are the exponential coefficients in the equation for velocity of edge dislocations. $ps$ and $qs$ are the exponential coefficients in the equation for velocity of screw dislocations. $F_0$ is the activation energy for edge dislocation motion (Alankar et al., 2011, 2009; Arsenlis and Tang, 2003; Arsenlis and Parks, 2002). $F_{0,kink}$ is the activation energy for the motion of screw dislocations via kink pair formation. $k_B$ is the Boltzmann constant. $\tau_{e,0}$ is the lattice friction acting on the motion of edge dislocations. $\tau_p$ is the Peierls stress (Stainier et al., 2003) on screw dislocations. $l_0$ is the critical kink nucleation length. $R_e^\chi$ and $R_s^\chi$ are the critical radii (Arsenlis and Parks, 2002) of interactions for edge and screw dislocations respectively.

$$S^\alpha = \mu b^\alpha \sqrt{\sum_\beta g^{\alpha\beta}(\rho_e^\beta \mathbf{n}^\alpha.\mathbf{t}_e^\beta + \rho_s^\beta \mathbf{n}^\alpha.\mathbf{t}_s^\beta)} \tag{5}$$

where $\mu$ is the shear modulus, $g^{\alpha\beta}$ is the latent hardening coefficient matrix for slip systems $\alpha$ and $\beta$. $\mathbf{n}^\alpha$ is the glide plane normal and $\mathbf{t}_e^\beta$ and $\mathbf{t}_s^\beta$ are the tangent directions of edge and screw dislocations on the forest slip system. The coefficients in this interaction matrix are chosen so that the hardening behavior generally reflects the salient features of the stress–strain response reported in the literature. The self interaction coefficient is assumed to be 40% lower (cf. Table 2) than the latent hardening coefficient. $\rho_e^\beta$ and $\rho_s^\beta$ are the edge and screw type dislocation densities on the forest slip systems.

### 2.4. Segment length

The average segment length of dislocations $l^\alpha$ on a mobile slip system $\alpha$ is given by the projection of forest dislocations on slip system $\beta$ (Alankar et al., 2011):

$$l^\alpha = \frac{\lambda}{\sqrt{\sum_\beta(\rho_e^\beta \mathbf{n}^\alpha.\mathbf{t}_e^\beta + \rho_s^\beta \mathbf{n}^\alpha.\mathbf{t}_s^\beta)}} \tag{6}$$

where $\rho_e^\beta$ and $\rho_s^\beta$ are the edge and screw type dislocation densities, respectively, on a forest slip system $\beta$. $\lambda$ is a proportionality coefficient to correlate the average dislocation segment length with the mean free path of the dislocations. For simplicity we assume this coefficient to be identical for edge and screw dislocations.

In this work we use our model approach primarily for performing a parametric study on the effect of different edge and screw dislocation velocities on giant plastic ansiotropy as described in terms of the Lankford value (also referred to as $r$-value). Initial model validation is conducted by the comparison of deformation texture predictions with experimental literature data. More detailed crystal plasticity simulations of α-Fe single crystals on the basis of the current model (see (Keh, 1965)) and the evolution of the crystallographic texture compared to experimental data will be presented in a subsequent work.

## 3. Simulation results and discussion

### 3.1. Evolution of crystallographic texture

The model described in Section 2 is employed as a user interface subroutine UMAT of ABAQUS (2005). The numerical integration of the constitutive equations is done as described in the Appendix of the work by Alankar et al. (2009). Initial validation of the model is conducted via simulations of the evolution of the crystallographic texture during plane strain compression of α-iron. For these simulations a cubic geometry is meshed by using 1728 elements that have 8 nodes and

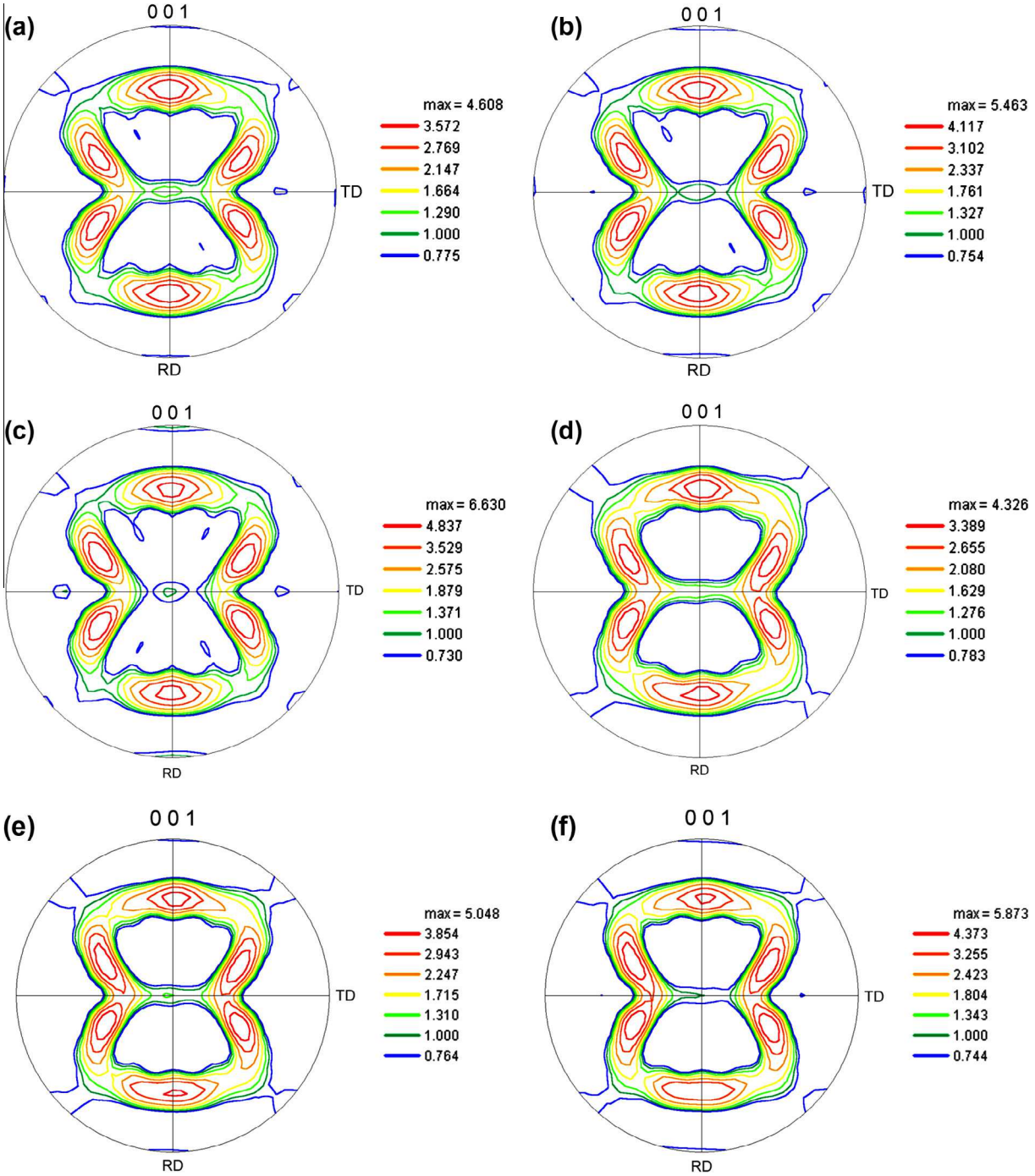


**Fig. 2.** Crystallographic texture evolution with 70–90% thickness reduction represented as {0 0 1} pole figures. For these simulations only iso-latent hardening is considered (no dislocation reaction based hardening coefficients). (a), (b), (c) represent the crystallographic texture evolution at 70 %, 80 % and 90 % deformation respectively by using first 12 slip systems in Table 1. (d), (e), (f) represent the crystallographic texture evolution by using all 24 slip systems in Table 1.

8 integration points each. Each element is considered as one grain. This setup altogether reproduces a random orientation distribution and is chosen as starting texture of the initial finite element mesh. As shown in Figs. 2 and 3, the model is able to predict the typical crystallographic texture evolution of α-iron during plane strain compression for thickness reductions of 70%, 80% and 90% (Hölscher et al., 1991, 1994; Huh et al., 1995; Hutchinson, 1999; Raabe and Lücke, 1993) that can be validated well against the experimental observations as reported in a standard book describing the crystallographic texture of metals e.g. Kocks et al., (2000).

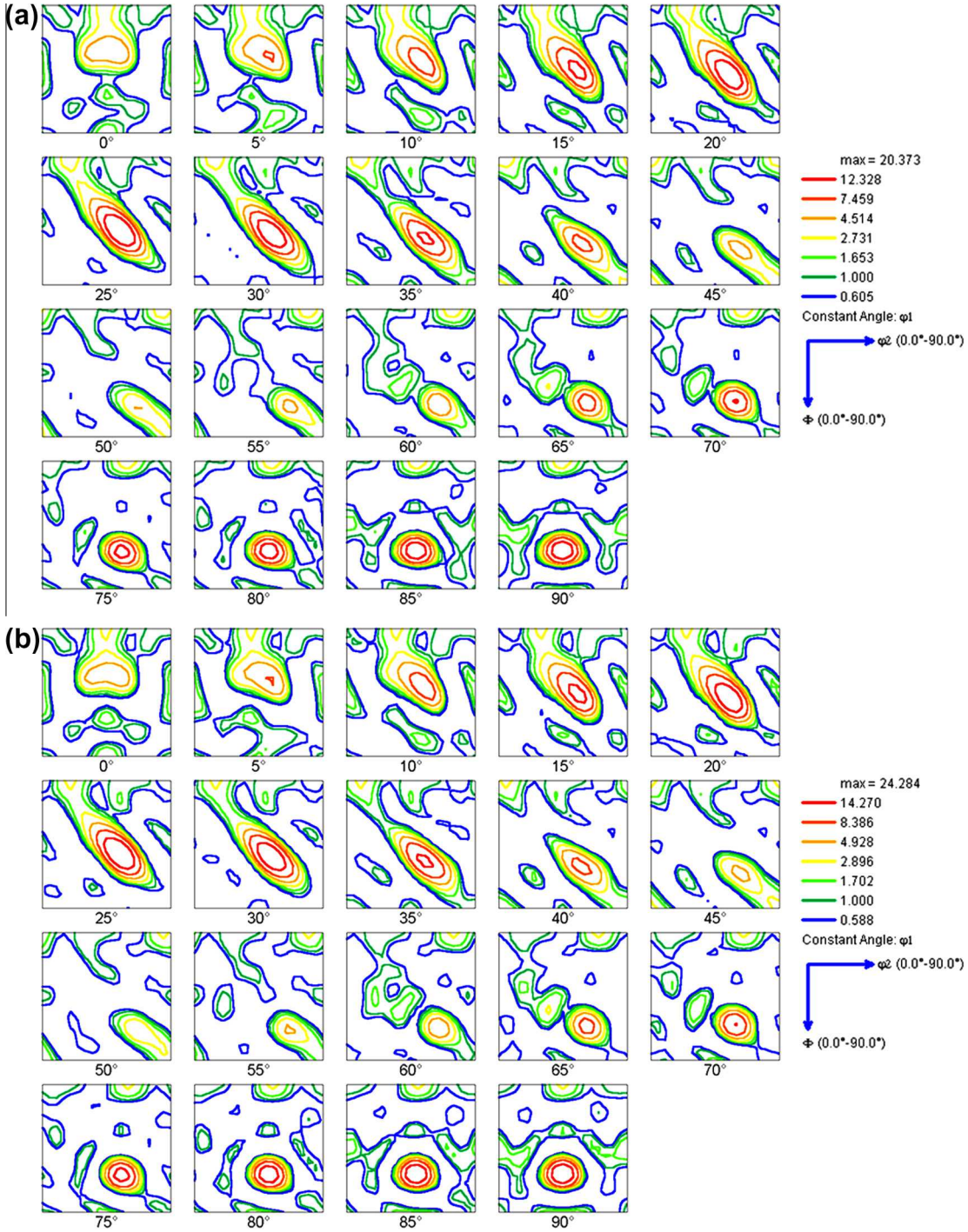


**Fig. 3.** Crystallographic texture evolution (ODFs: orientation distribution functions) with increasing thickness reduction. For these simulations only isolatent hardening is considered (i.e. no dislocation reaction based hardening coefficients are considered). (a), (b), (c) represent the crystallographic texture evolution at 70 %, 80 % and 90 % deformation respectively by using first 12 slip systems in Table 1. (d), (e), (f) represent the crystallographic texture evolution by using all 24 slip systems in Table 1.

### *3.2. Evolution of r-value in electro-deposited pure iron*

In this section we apply the constitutive model in order to understand extreme plastic anisotropy effects in terms of the *r*-value (Lankford-value) in electrodeposited $\alpha$-iron sheet. The *r*-value describes the ratio between the in-plane deformation component and the deformation component in through-thickness direction. This means that a high *r*-value describes mate-

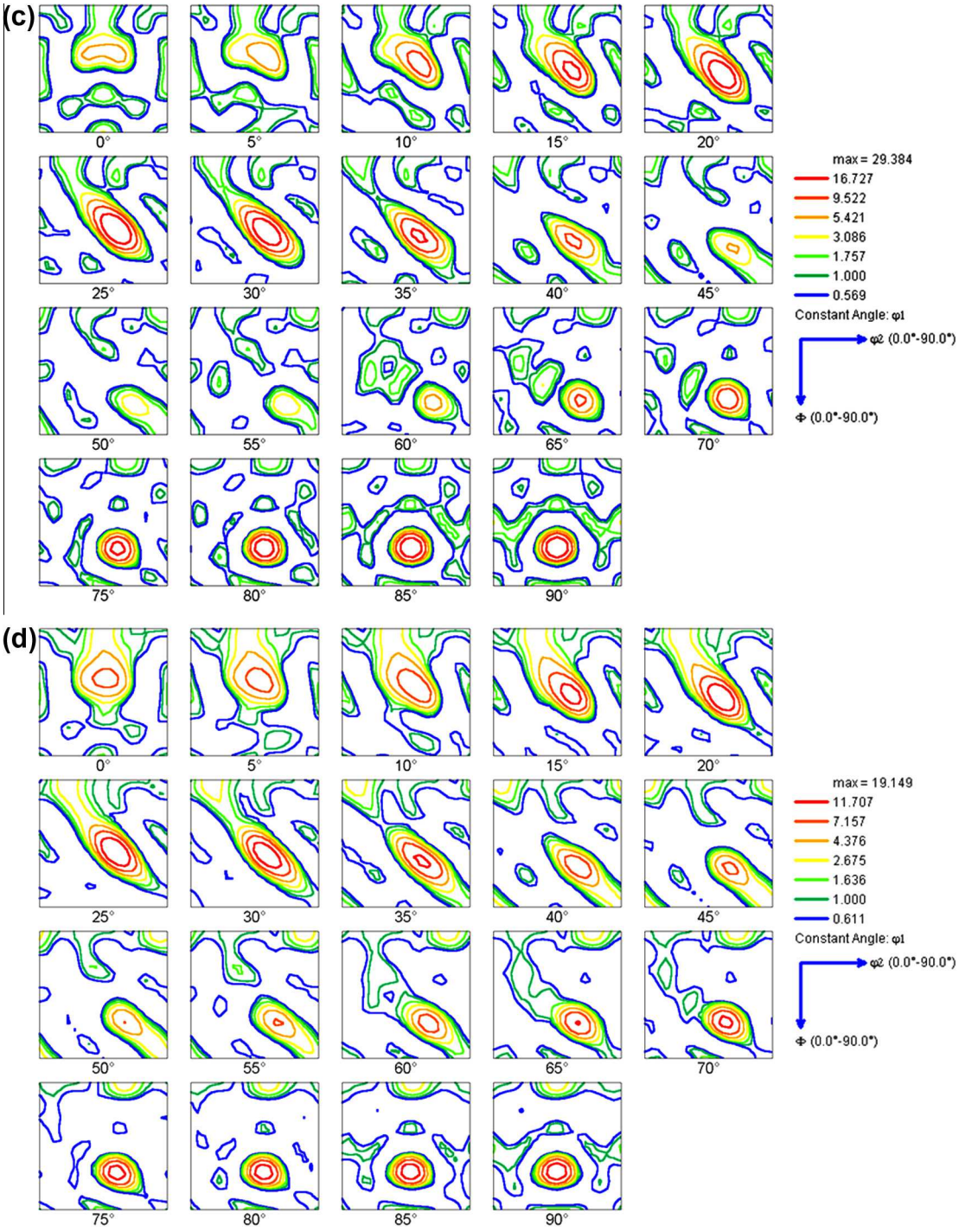


**Fig. 3.** (*continued*)

rial flow primarily parallel to the plane surface in drawing or stretching operation while a low *r*-value indicates a high portion of normal flow. The former effect (high *r*-value) indicates good formability in sheet forming operations while the latter effect (low *r*-value) indicates rapid sheet thinning leading potentially to premature localization and failure.

As mentioned above, it was observed that electro-deposited pure α-iron having extremely sharp <1 1 1>//ND crystallographic texture shows a very high *r*-value (ND: normal direction). An experimental assessment reported by Yoshinaga et al. (2008) shows *r*-values ranging from 4.8 to 7.1 (see Fig. 5 in Yoshinaga et al. (2008)) for different electro-deposited pure

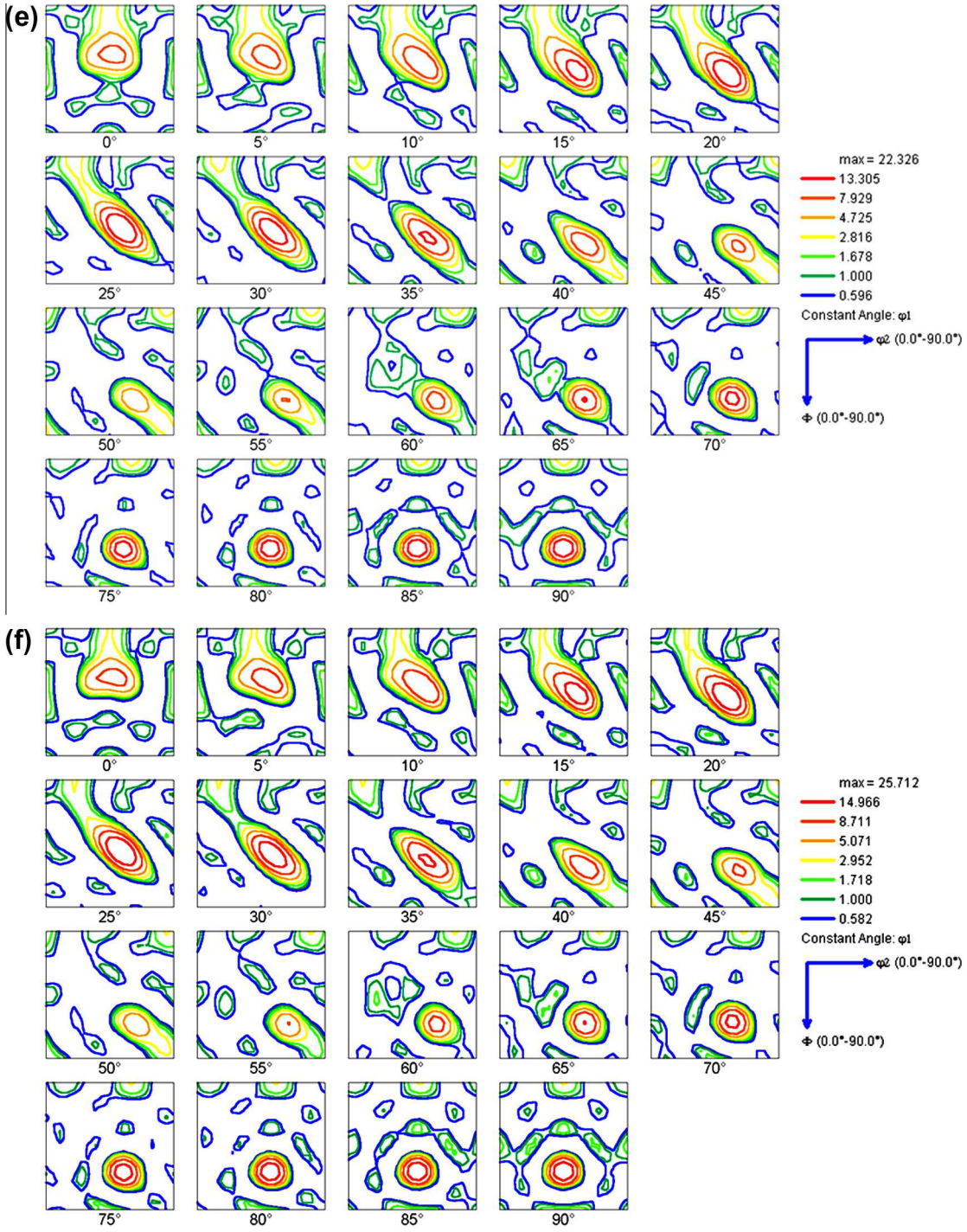


**Fig. 3.** (*continued*)

iron sheets. These values are much higher than those observed in the best interstitial free IF sheet steels which are characterized by *r*-values ranging from 1.4 to 2.7 (Yoshinaga et al., 2008). Calculations performed by Yoshinaga et al. (2008) using different Taylor-Bishop-Hill type isostrain (Taylor Full Constraints model, FC) and relaxed isostrain (Taylor Relaxed Constraints model, RC) homogenization models (Van Houtte, 1988) do not predict *r*-values above 3.2. The FC and RC models that the authors used for the analysis did not incorporate any details of the microstructure such as dislocation density based strain hardening or appropriate dislocation velocity laws. As mentioned earlier in Section 2, the crystal plasticity model that

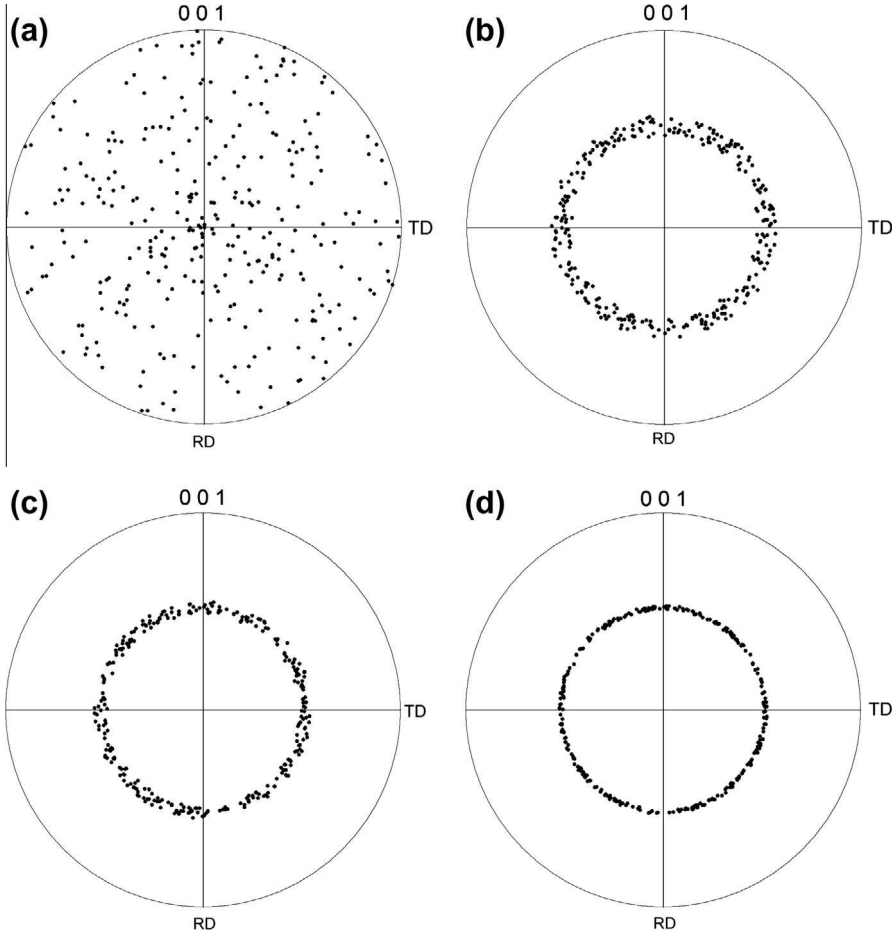


**Fig. 4.** Various initial orientation distributions used in the simulation study on plastic anisotropy. (a) 100 randomly distributed orientations; γ fiber (<1 1 1>//ND) orientations described by (b) 100 orientations with 5° misorientation from the ideal <1 1 1>//ND; (c) 100 orientations with 3° misorientation from the ideal <1 1 1>//ND; and (d) 100 orientations with 1° misorientation from the ideal <1 1 1>//ND (ND: normal direction).

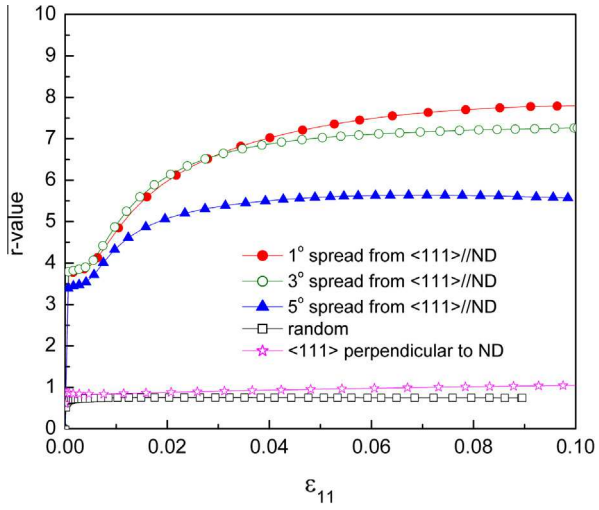


**Fig. 5.** Evolution of the predicted *r*-values as a function of the uniaxial strain in a simulated tensile test for varying sharpness of the initial <1 1 1>//ND texture. In these simulations only multiplication of dislocations was assumed i.e. dislocation annihilation was turned off in order to mimic the effect of the longitudinal needle shaped grain shapes.

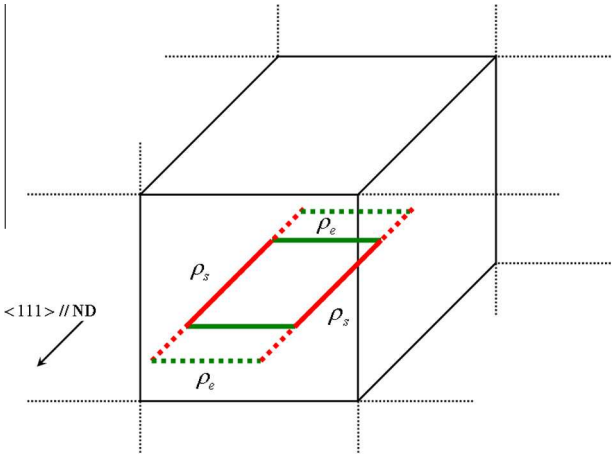


**Fig. 6.** A dislocation loop expanding under the effect of applied stress in one of the grains oriented such that <1 1 1>//ND. In such grains, it is highly probable that most of the screw dislocation lines are aligned along the ND with slight misorientation.

we are introducing in this work uses such fundamental microstructure variables as it is based on dislocation mechanisms in a bcc crystal. One should note though that in the simulations for determining *r*-values we use only 12 <1 1 1>[1 1 0] slip systems like Yoshinaga et al., (2008).

We define the initial crystallographic texture as (a) 'random'; (b) 5° misorientation from the ideal <1 1 1>//ND; (c) 3° misorientation from the ideal <1 1 1>//ND (d); and 1° misorientation from the ideal <1 1 1>//ND. The pole figures representing these initial crystallographic textures are shown in Fig. 4.

The orientations shown in Fig. 4 are assigned to a block of 100 elements (8 node brick elements – C3D8 as defined in the ABAQUS$^{TM}$ (2005) Standard library). For all simulations standard displacement boundary conditions are applied in order to describe a uniaxial tensile test for a total strain of 10% in tensile direction. Fig. 5 shows the evolution of predicted *r*-value for the different initial crystallographic textures as a function of the total tensile strain. Note that for accounting for the effect of needle shaped highly elongated grains (see Fig. 2 in Yoshinaga et al. (2008)) we turn off the annihilation of dislocations in the model (i.e. $R_e = R_s = 0$ in Eqs. (3a) and (3b) respectively). The results reveal that with decreasing average misorientation from the ideal <1 1 1> axis, the *r*-value increases and is extremely large as compared with the one determined for the case with an initially random texture (*r*-value $\sim$ 1.0). Our simulation results are profoundly different from the FC and RC simulation results reported by Yoshinaga et al. (2008). Besides the large differences in magnitude of *r*-values from our simulation results compared to the values simulated by Yoshinaga et al. (2008) we predict that the *r*-values are also functions of the gradually evolving crystallographic texture. This is reasonable as the *r*-value is a function of crystallographic orientation. Similar to Yoshinaga et al. (2008), we discuss the *r*-value at 10% uniaxial tensile strain. For the orientations that have 5°, 3° and 1° average misorientation, respectively, from the ideal <1 1 1>//ND texture, the *r*-values are $\sim$5.6, 7.2, and 7.6 respectively after 10% strain. If the annihilation of the dislocations is not turned off in the constitutive description i.e. $R_e$ and $R_s$ are not set to zero in Eqs. (3a) and (3b), respectively, than the *r*-value does not become so high. For example, for 1° misorientation from the <1 1 1>//ND texture, the *r*-value decreases from $\sim$7.6 to $\sim$6.5 at 10% strain in this case. These results indicate that in large grains in which dislocations can substantially annihilate before reaching grain boundaries, the *r*-value will not be as high as in long needle-shaped grains.

Further, we explain this unexpected phenomenon of large *r*-values in terms of dislocation loop activities in the needle shaped grains. As mentioned earlier, in $\alpha$-Fe, edge dislocations move much faster than screw dislocations. Owing to this kinetic constraint, the best possible accommodating expansion of such dislocation loops should be the one in which screw dislocation segments are oriented along the larger dimension of the needle shaped grains. This arrangement allows the maximum unrestricted glide of edge and screw dislocations according to their velocities. Such shape of dislocation loops arises necessarily when accounting for the different glide rates of the two types of dislocations. Fig. 6 schematically shows one of the long grains having strong <1 1 1>//ND texture formed during the electrodeposition of $\alpha$-Fe (Yoshinaga et al., 2008). Formability is interpreted as the ability of a metal to undergo severe shape changes without fracture. In terms of dislocation theory, better formability means the ability to deform without redundant interaction of dislocations. In the present case, the redundant interaction of dislocations is bypassed due to the fact that accommodating glide paths available to the edge and screw dislocations, as prescribed by the grain shapes, are matching their natural expansion in accord with their individual velocities. Therefore such a combination of dislocation velocities ($\bar{v}_e^{\alpha} > \bar{v}_s^{\alpha}$), crystallographic <1 1 1> texture, and elongated grain shapes consequently enables enhanced formability. Specifically under these crystallographic and topological boundary conditions the alignment of the screw dislocations is parallel to the longitudinal axis of the needle shaped grains. One should note that for bcc metals we essentially do not need to turn off the annihilation of screw dislocations since their velocity is already so low that they will not undergo substantial annihilation. For achieving a similar case for fcc crystals it is necessary to (artificially) turn off the annihilation of both edge and screw dislocations in the model.

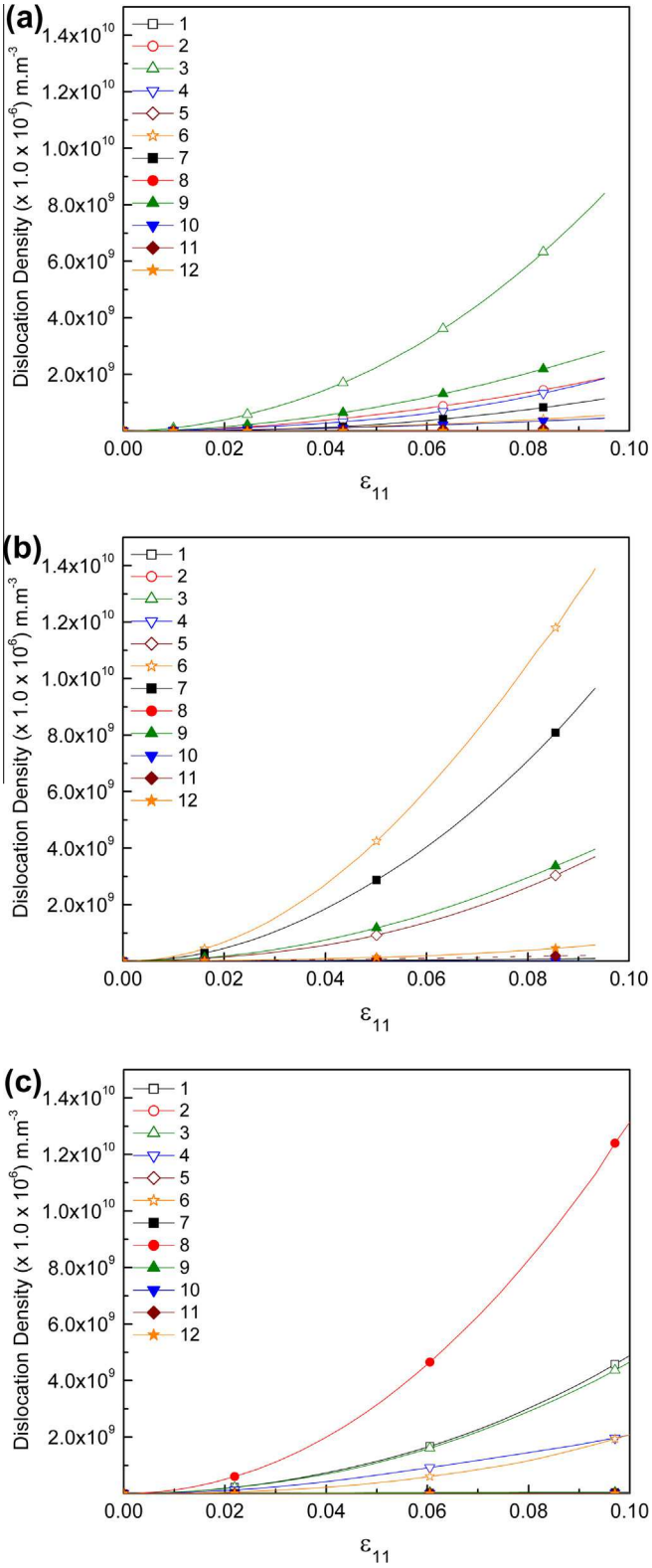


**Fig. 7.** Slip system activity in the simulations with (a) 1° misorientation from the ideal <1 1 1>//ND; (b) 3° misorientation from the ideal <1 1 1>//ND; and (c) 5° misorientation from the ideal <1 1 1>//ND fiber orientation (ND: normal direction). The numbers 1, 2, 3 . . . indicate the individual slip systems according to Table 1.

The physical interpretation of these simulation results is given in terms of the underlying slip systems and their kinetics. Fig. 6 shows a dislocation loop expanding under the effect of the applied stress in one of the grains oriented such that the crystal <1 1 1> direction aligns with the normal direction of the tensile sample (ND). In such grains, it is highly probable that most of the screw dislocation lines are aligned along ND with the slight misorientation scatter used as a parameter as described above. By decreasing the misorientation from <1 1 1>//ND it is ensured that the slip systems available in the grains are the ones which have 111-screw dislocations along the length of the grains. One should note that the grains have a strong <1 1 1>//ND texture so there is very small probability of other slip systems to become critically stressed. Our simulations show that in most of the grains ~4 slip systems are active in such a case and this number of slip systems decreases as the misorientation relative to the <1 1 1> axis decreases (cf. Fig. 7). This effect decreases the amount of latent hardening and most of the hardening affecting the deformation is due to the interaction of dislocations with grain boundaries after a long and undisturbed mean free glide path. The interaction of grain boundaries with these dislocations is not included in the constitutive model though, but the effect of different mobilities of edge and screw dislocations on the formability is obvious. Note in Fig. 7, that the dislocation density evolution rate and total dislocation density at 10% tensile strain is very high since for replicating the effect of needle shaped grains we do not account for annihilation of dislocations ($R_e = R_s = 0$ in Eqs. (3a) and (3b)). With an increase in the misorientation of the starting texture away from the ideal <1 1 1> ND axis, more and more slip systems become active and higher strain hardening takes place. The increase in strain hardening in turn is reflected by the decreased $r$-value for those simulations that start with larger average misorientations of the grains from the ideal <1 1 1> axis.

In the present case, the orientation of the screw dislocations is such that there is very low resolved shear stress on the screw dislocations. This low available shear stress and high Peierls stress make the movement and therefore annihilation of screw dislocations very difficult. The effect of annihilation of edge dislocation segments will not be strong since they are much smaller in length. However, due to high velocity of edge dislocation segments, the length of screw dislocation segments will increase quickly. This effect causes more multiplication of dislocations than the effect of annihilation if any. A similar effect of the annihilation of dislocations is shown in Fig. 8. The lowest $r$-values are achieved when regular annihilation of dislocations is taking place ($R_e = R_s \neq 0$ in Eqs. (3a) and (3b)). In Fig. 8, we study the effect of the individual dislocation velocities and the different conditions of annihilation of the dislocations for grain orientations which are oriented within 5° misorientation from <1 1 1>//ND. Interestingly, for a 5° spread of the orientations away from the ideal <1 1 1>//ND texture, the highest $r$-value is seen when the annihilation of dislocations is (artificially) turned off ($R_e = R_s = 0$ in Eqs. (3a) and (3b) respectively) and the velocities of the edge and screw dislocations are identical $v_e = v_s$. This constitutive rule mimics a topological situation of long needle shaped grains for bcc crystals being deformed at high temperature where no friction barrier acts against the free motion of screw dislocations (Seeger, 2001) and dislocation annihilation is not taking place. Note that if $R_e$ and $R_s$ are not set to zero then the $r$-value is not that high ($R_e$ and $R_s$ indicate the critical interaction radii for edge and screw type dislocations respectively). This result is shown by the pink curve in Fig. 8.

Finally, the overall effect on $r$-value can be described as a type of grain topology or, more specific, grain-shape effect. In the present case it is shown that this effect is built-in into the microstructure and is an outcome of the dislocation mean free path and the different velocities of edge and screw dislocations in a bcc crystal. The $r$-values that we predict with this approach are in good agreement with the experimental data (4.1–7.0) (Yoshinaga et al., 2008). From our approach we can specifically learn that such macroscopic quantities as the Lankford anisotropy factor ($r$-value) can depend to a large degree not

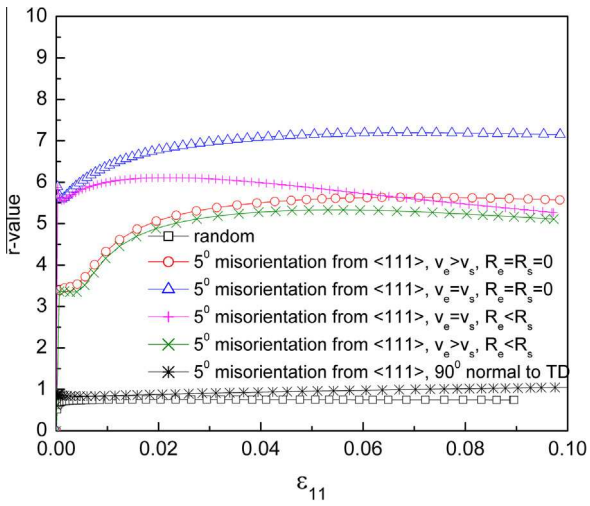


**Fig. 8.** Effect of dislocation velocity and dislocation density evolution on the evolution of the $r$-value. $R_e$ and $R_s$ represent the critical interaction radii for edge and screw dislocations respectively as defined in Eq. (3). $v_e$ and $v_s$ are velocities of edge and screw dislocations respectively.

only on the crystallographic texture but also on the underlying dislocation kinetics. This is reflected by Yoshinaga's work (Yoshinaga et al., 2008) who suggested that the observed giant planar anisotropy could not be modeled by using traditional micromechanical homogenization approaches (FC, RC Taylor models) alone (Van Houtte, 1988) although they served well over several decades for describing certain features of the crystallographic texture evolution. However, instead the authors suggested that more flexible constitutive models should be developed which would be then able, for instance, to predict the high *r*-values in electro-deposited pure iron sheets having long needle shaped grains. Delannay and Barnett (2011), recently, have attempted to model such plastic anisotropy based on explicit modeling of the grain size and grain shape by using a phenomenological crystal plasticity model.

## 4. Conclusions

We present a physically based crystal plasticity model for finite deformation of bcc crystals. The novelty of the constitutive approach is that it considers the individual kinetics of screw and edge dislocations that can lead to the formation of characteristic dislocation loops in a bcc crystal. The constitutive framework is self sustained and does not require the commonly used power law formulations. More specifically the model distinguishes between the edge and screw dislocations via different velocities of the two types of dislocations in a bcc crystal. The velocity of the screw dislocations is accounted by the formation of kink-pairs. The model is able to predict the evolution of the crystallographic texture reasonably well. We use the model for predicting the excellent formability in terms of the *r*-value of electro-deposited pure iron which has a strong <1 1 1>//ND texture. The model shows excellent predictions of the *r*-value as compared with experiments. The *r*-value increases with decreasing misorientation of the average grain orientation from the ideal <1 1 1>//ND axis. This effect cannot be so well predicted by the model without accounting for different velocities of edge and screw type dislocations and also not without turning off the annihilation of the dislocations (due to low velocity of screw dislocations). A major advantage of the models like the one presented here is that their modular nature enables us to include also further deformation mechanism at the generic dislocation level. The work gives an example of the fact that models that are based on fundamental dislocation mechanisms in crystal plasticity, are suited not only for understanding the underlying physics at the single dislocation level but they also can replace more traditional homogenization approaches that rely on phenomenological power-law formulations.

## References


ABAQUS Reference Manual Versions 6.5. ABAQUS Inc., Providence, RI.

Acharya, A., Chapman, S.J., 2012. Elementary observations on the averaging of dislocation mechanics: dislocation origin of aspects of anisotropic yield and plastic spin. Proc. IUTAM 3, 301–313.

Adams, J.J., Agosta, D.S., Leisure, R.G., Ledbetter, H., 2006. Elastic constants of monocrystal iron from 3 to 500 K. J. App. Phys. 100, 113530-1–113530-7.

Akhtar, A., Teghtsoonian, E., 1975. Prismatic slip in alpha-titanium single crystals. Metall. Mater. Trans. A 6, 2201–2208.

Alankar, A., Field, D.P., 2012. Modeling of deformation microstructure–strain hardening and crystallographic reorientation of crystallites in a columnar polycrystal. Mater. Sci. Forum 702–703, 196–199.

Alankar, A., Mastorakos, I.N., Field, D.P., 2009. A dislocation-density-based 3D crystal plasticity model for pure aluminum. Acta Mater. 57, 5936–5946.

Alankar, A., Eisenlohr, P., Raabe, D., 2011. A dislocation density-based crystal plasticity constitutive model for prismatic slip in a-titanium. Acta Mater. 59, 7003–7009.

Alankar, A., Field, D.P., Zbib, H.M., 2012a. Explicit incorporation of cross-slip in a dislocation density based crystal plasticity model. Philos. Mag. 92, 3084–3100.

Alankar, A., Mastorakos, I.N., Field, D.P., Zbib, H.M., 2012b. Determination of dislocation interaction strengths using discrete dislocation dynamics of curved dislocations. J. Eng. Mater. Technol. 134, 021014–021018.

Aoyagi, O., Kobayashi, R., Kaji, Y., Shizawa, K., 2013. Modeling and Simulation on Ultrafine-graining Based on Multiscale Crystal Plasticity Considering Dislocation Patterning. Int. J. Plast. 47, 13–28.

Arsenlis, A., Parks, D.M., 2002. Modeling the evolution of crystallographic dislocation density in crystal plasticity. J. Mech. Phys. Solids 50, 1979–2009.

Arsenlis, A., Tang, M., 2003. Simulations on the growth of dislocation density during stage 0 deformation in BCC metals. Model. Simul. Mater. Sc. 11, 251–264.

Austin, R., McDowell, D.L., 2011. A dislocation-based constitutive model for viscoplastic deformation of fcc metals at very high strain rates. Int. J. Plast. 27, 1–24.

Barrett, C.S., Ansel, G., Mehl, R.F., 1937. Trans. Am. Soc. Metall. 25, 702–733.

Beaudoin, A.J., Mathur, K.K., Dawson, P.R., Johnson, G.C., 1993. Three-dimensional deformation process simulation with explicit use of polycrystal plasticity models. Int. J. Plast. 9, 833–860.

Beaudoin, A.J., Dawson, P.R., Mathur, K.K., Kocks, U.F., Korzekwa, D.A., 1994. Application of polycrystal plasticity to sheet forming. Comput. Methods Appl. Mech. Eng. 117, 49–70.

Cai, W., 2001. Atomistic and Mesoscale Modeling of Dislocation Mobility. Massachesetts Institute of Technology.

Chen, N.K., Maddin, R., 1954. Geometrical aspect of the plastic deformation of metal single crystals. Acta Metall. 2, 49–51.

Cheong, K.-S., Busso, E.P., 2004. Discrete dislocation density modelling of single phase FCC polycrystal aggregates. Acta Mater. 52, 5665–5675.

Delannay, L., Barnett, M.R., 2011. Modelling the combined effect of grain size and grain shape on plastic anisotropy of metals. Int. J. Plast. 32–33, 70–84.

Devincre, B., Hoc, T., Kubin, L., 2008. Dislocation mean free paths and strain hardening of crystals. Science 320, 1745–1748.

Dorn, J.E., Rajnak, S., 1964. Nucleation of kink pairs and the peierls' mechanism of plastic deformation. Trans. Metal. Soc. AIME 230, 1052.

Duesbery, M.S., 1969. The influence of core structure on dislocation mobility. Philos. Mag. A 19, 501–526.

Erieau, P., Rey, C., 2004. Modeling of deformation and rotation bands and of deformation induced grain boundaries in IF steel aggregate during large plane strain compression. Int. J. Plast. 20, 1763–1788.

Evers, L.P., Brekelmans, W.A.M., Geers, M.G.D., 2004. Scale dependent crystal plasticity framework with dislocation density and grain boundary effects. Int. J. Solids Struct. 41, 5209–5230.

Field, D.P., Alankar, A., 2011. Observation of deformation and lattice rotation in a Cu bi-crystal. Met. Metall. Trans. A. 42, 676–683.

Franciosi, P., Berveiller, M., Zaoui, A., 1980. Latent hardening in copper and aluminum single crystals. Acta Metall. 28, 273–283.

Gough, H.J., 1928. The behavior of a single crystal of alpha-iron subjected to alternating torsional stresses. Proc. R. Soc. London A 118, 498–534.

Guyot, P., Dorn, J.E., 1967. A critical review of the Peierls' mechanism. Can. J. Phys. 45, 983.
Han, C., Ma, A., Roters, F., Raabe, D., 2007. A finite element approach with patch projection for strain gradient formulations. Int. J. Plast. 23, 690–710.
Hirth, J.P., Hoagland, R.G., 1993. Nonlinearities in the static energetics and in the kinematics of dislocations. Physica D 66, 71–77.
Hirth, J.P., Lothe, J., 1992. Theory of Dislocations. McGraw-Hill, New York.
Hölscher, M., Raabe, D., Lücke, K., 1991. Rolling and recrystallization textures of bcc steels. Steel Res. 62, 567–575.
Hölscher, M., Raabe, D., Lücke, K., 1994. Relationship between rolling textures and shear textures in f.c.c. and b.c.c. metals. Acta Metall. 42, 879–886.
Huh, M.-Y., Raabe, D., Engler, O., 1995. On the influence of solution treatment on the microstructure and crystallographic texture of cold rolled and recrystallised low carbon steel. Steel Res. 66, 353–359.
Hutchinson, B., 1999. Deformation microstructures and textures in steels. Philos. Trans. R. Soc. London A 357, 1471–1485.
Ito, K., Vitek, V., 2001. Atomistic study of non-Schmid effects in the plastic yielding of bcc metals. Philos. Mag. A 81, 1387–1407.
Kalidindi, S.R., Schoenfeld, S.E., 2000. On the prediction of yield surfaces by the crystal plasticity models for fcc polycrystals. Mater. Sci. Eng. A 293, 120–129.
Keh, A.S., 1965. Work hardening and deformation sub-structures in iron single crystals deformed in tension at 298 degrees K. Philos. Mag. 12, 9–30.
Kitayama, K., Tomé, C.N., Rauch, E.F., Gracio, J.J., Barlat, F., 2012. A crystallographic dislocation model for describing hardening of polycrystals during strain path changes. Application to low carbon steels. Int. J. Plast. 46, 54–69.
Kocks, U.F., Tome, C.N., Wenk, H.-R., 2000. Texture and anisotropy–preferred orientations in polycrystals and their effect on materials properties. Cambridge University Press.
Kubin, L.P., Devincre, B., Tang, M., 1998. Mesoscopic modelling and simulation of plasticity in fcc and bcc crystals: dislocation intersections and mobility. J. Comput.-Aided Mater. Des. 5, 31–54.
Lee, Y.J., Subhash, G., Ravichandran, G., 1999. Constitutive modeling of textured body-centered-cubic (bcc) polycrystals. Int. J. Plast. 15, 625–645.
Lim, H., Lee, M.G., Kim, J.H., Adams, B.L., Wagoner, R.H., 2011. Simulation of polycrystal deformation with grain and grain boundary effects. Int. J. Plast. 27, 1328–1354.
Ma, A., Roters, F., Raabe, D., 2006. On the consideration of interactions between dislocations and grain boundaries in crystal plasticity finite element modeling – theory, experiments, and simulations. Acta Mater. 54, 2181–2194.
Ma, A., Roters, F., Raabe, D., 2007. A dislocation density based constitutive law for BCC materials in crystal plasticity FEM. Comput. Mater. Sci. 39, 91–95.
Madec, R., Kubin, L.P., 2003. Dislocation interactions and symmetries in BCC crystals. In: Kitagawa, H., Shibutani, Y. (Eds.), IUTAM Symposium on Mesoscopic Dynamics of Fracture Process and Materials Strength. Springer, Osaka, Japan, p. 476.
Mayeur, J.R., McDowell, D.L., Bammann, D.J., 2011. Dislocation-based micropolar single crystal plasticity: comparison of multi- and single criterion theories. J. Mech. Phys. Solids 59, 398–422.
Monnet, G., Devincre, B., Kubin, L.P., 2004. Dislocation study of prismatic slip systems and their interactions in hexagonal close packed metals: application to zirconium. Acta Mater. 52, 4317–4328.
Neale, K.W., 1993. Use of crystal plasticity in metal forming simulations. Int. J. Mech. Sci. 35, 1053–1063.
Ortiz, M., Repetto, E.A., Stainier, L., 2000. A theory of subgrain dislocation structures. J. Mech. Phys. Solids 48, 2077–2114.
Queyreau, S., Monnet, G., Devincre, B.t., 2009. Slip systems interactions in Î±-iron determined by dislocation dynamics simulations. Int. J. Plast. 25, 361–377.
Raabe, D., 1995. Simulation of rolling textures of bcc metals under consideration of grain interactions and {110}, {112 and {123} slip planes. Mater. Sci. Eng. A 197, 31–37.
Raabe, D., Lücke, K., 1993. Textures of ferritic stainless steels. Mater. Sci. Technol. 9, 302–312.
Raabe, D., Roters, F., 2004. Using texture components in crystal plasticity finite element simulations. Int. J. Plast. 20, 339–361.
Raabe, D., Wang, Y., Roters, F., 2005. Crystal plasticity simulation study on the influence of texture on earing in steel. Comput. Mater. Sci. 34, 221–234.
Raphanel, J.L., Van Houtte, P., 1985. Simulation of the rolling textures of b.c.c. metals by means of the relaxed taylor theory. Acta Metall. 33, 1481–1488.
Roters, F., Eisenlohr, P., Hantcherli, L., Tjahjanto, D.D., Bieler, T.R., Raabe, D., 2010. Overview of constitutive laws, kinematics, homogenization and multiscale methods in crystal plasticity finite-element modeling: theory, experiments, applications. Acta Mater. 58, 1152–1211.
Seeger, A., 2001. Why anomalous slip in body-centered cubic metals. Mater. Sci. Eng. A 319–321, 254–260.
Seeger, A., Schiller, P., 1962. The formation and diffusion of kinks as the fundamental process of dislocation movement in internal friction measurements. Acta Metall. 10, 348.
Segurado, J., Lebensohn, R.A., Llorca, J., Tome, C.N., 2012. Multiscale modeling of plasticity based on embedding the viscoplastic self-consistent formulation in implicit finite elements. Int. J. Plast. 28, 124–140.
Sesták, B., Seeger, A., 1978a. Glide and work-hardening in bcc-metals and alloys.1. Z. Metallkunde 69, 195–202.
Sesták, B., Seeger, A., 1978b. Glide and work-hardening in bcc-metals and alloys.2. Z. Metallkunde 69, 355–363.
Shanthraj, P., Zikry, M.A., 2011. Dislocation density evolution and interactions in crystalline materials. Acta Mater. 59, 7695–7702.
Srivastava, K., Gröger, R., Weygand, D., Gumbsch, P., 2013. Dislocation motion in tungsten: atomistic input to discrete dislocation simulations. Int. J. Plast. 47, 126–142.
Stainier, L., Cuitino, A.M., Ortiz, M., 2002. A micromechanical model of hardening, rate sensitivity and thermal softening in BCC single crystals. J. Mech. Phys. Solids 50, 1511–1545.
Stainier, L., Cuitino, A.M., Ortiz, M., 2003. Multiscale modelling of hardening in BCC crystal plasticity. J. Phys. IV France 105, 157–164.
Tang, M., Kubin, L.P., Canova, G.R., 1998. Dislocation mobility and the mechanical response of b.c.c. single crystals: a mesoscopic approach. Acta Mater. 46, 3221–3235.
Taylor, G.I., 1928. The deformation of crystals of beta-brass. Proc. R. Soc. A London 118, 1.
Tikhovskiy, I., Raabe, D., Roters, F., 2008. Simulation of earing of a 17% Cr stainless steel considering texture gradients. Mater. Sci. Eng. A 488, 482–490.
Van Houtte, P., 1988. Textures Microstruct. 8–9, 313.
Vitek, V., 1974. Theory of the core structures of dislocations in body-centered cubic metals. Cryst. Latt. Def. 5, 1.
Vitek, V., 1976. Computer simulation of the screw dislocation motion in bcc metals under the effect of the external shear and uniaxial stresses. Proc. R. Phys. Soc. A352, 109.
Xie, C.L., Nakamachi, E., 2002. Investigations of the formability of BCC steel sheets by using crystalline plasticity finite element analysis. Mater. Des. 23, 59–68.
Xu, W., Moriarty, J.A., 1998. Accurate atomistic simulations of the peierls barrier and kink-pair formation energy for <1 1 1> screw dislocation in bcc Mo. Comput. Mater. Sci. 9, 348–356.
Yoshida, K., Ishizaka, T., Kuroda, M., Ikawa, S., 2007. The effects of texture on formability of aluminum alloy sheets. Acta Mater. 55, 4499–4506.
Yoshinaga, N., Sugiura, N., Hiwatashi, S., Ushioda, K., Kada, O., 2008. Deep drawability of electro-deposited pure iron having an extremely sharp <111>//ND texture. ISIJ Int. 48, 667–670.
Zhao, Z., Mao, W., Roters, F., Raabe, D., 2001. Introduction of a texture component crystal plasticity finite element method for anisotropy simulations. Adv. Eng. Mater. 3, 984–990.